materials

MDPI

Article

Reinforcing Increase of ΔT_c in MgB_2 Smart Meta-Superconductors by Adjusting the Concentration of Inhomogeneous Phases

Yongbo Li, Guangyu Han, Hongyan Zou, Li Tang, Honggang Chen and Xiaopeng Zhao *

Smart Materials Laboratory, Department of Applied Physics, Northwestern Polytechnical University, Xi'an 710072, China; 2014100616@mail.nwpu.edu.cn (Y.L.); guangyu@mail.nwpu.edu.cn (G.H.); 2019202522@mail.nwpu.edu.cn (H.Z.); 2018202416@mail.nwpu.edu.cn (L.T.); 2017100698@mail.nwpu.edu.cn (H.C.)

* Correspondence: xpzhao@nwpu.edu.cn

Abstract: Incorporating with inhomogeneous phases with high electroluminescence (EL) intensity to prepare smart meta-superconductors (SMSCs) is an effective method for increasing the superconducting transition temperature (T_c) and has been confirmed in both MgB_2 and Bi(Pb)SrCaCuO systems. However, the increase of ΔT_c ($\Delta T_c = T_c - T_{cpure}$) has been quite small because of the low optimal concentrations of inhomogeneous phases. In this work, three kinds of MgB_2 raw materials, namely, $^aMgB_2$, $^bMgB_2$, and $^cMgB_2$, were prepared with particle sizes decreasing in order. Inhomogeneous phases, Y_2O_3:Eu^{3+} and Y_2O_3:Eu^{3+}/Ag, were also prepared and doped into MgB_2 to study the influence of doping concentration on the ΔT_c of MgB_2 with different particle sizes. Results show that reducing the MgB_2 particle size increases the optimal doping concentration of inhomogeneous phases, thereby increasing ΔT_c. The optimal doping concentrations for $^aMgB_2$, $^bMgB_2$, and $^cMgB_2$ are 0.5%, 0.8%, and 1.2%, respectively. The corresponding ΔT_c values are 0.4, 0.9, and 1.2 K, respectively. This work open a new approach to reinforcing increase of ΔT_c in MgB_2 SMSCs.

Keywords: MgB_2; EL inhomogeneous phase; inject energy; SMSCs; ΔT_c

Citation: Li, Y.; Han, G.; Zou, H.; Tang, L.; Chen, H.; Zhao, X. Reinforcing Increase of ΔT_c in MgB_2 Smart Meta-Superconductors by Adjusting the Concentration of Inhomogeneous Phases. *Materials* **2021**, *14*, 3066. https://doi.org/10.3390/ma14113066

Academic Editors: Yong Seung Kwon and Andres Sotelo

Received: 1 May 2021
Accepted: 2 June 2021
Published: 4 June 2021

1. Introduction

According to BCS theory, McMillan theoretically calculated the upper limit of the critical temperature (T_c) of conventional BCS superconductors to be 40 K, which is called the McMillan limit temperature [1,2]. Although the T_c of conventional superconductors has an upper limit, the search for high-T_c superconducting materials has been continuous. High-temperature superconductors [3,4], iron-based superconductors [5,6], high-pressure superconductors [7–10], and photo-induced superconductors [11,12] have been gradually studied and discovered. However, these new superconducting materials are not simple conventional superconductors. Breaking the McMillan limit temperature remains a challenge for conventional BCS superconductors. In 2001, the superconductivity of MgB_2 was discovered [13]. The excellent superconductivity, simple preparation process, and especially high T_c of MgB_2 quickly aroused great interest in the scientific community and led scholars to believe that the McMillan limit temperature may finally be surpassed [14–19]. Various methods have been applied to improve the superconductivity of MgB_2 [20–24], which would not only improve the practical application of MgB_2 but also help transcend the McMillan limit temperature and further elucidate the superconducting mechanism. Chemical doping is often used to study superconductivity. Unfortunately, many experimental results confirm that this method reduces the T_c of MgB_2 [25–30]. Thus far, no useful strategy for improving the T_c of MgB_2 is yet available.

Metamaterial mainly refers to materials made up of two or more media, which can produce new properties that are not found in a single medium. Meta-method is often used to achieve some special properties and provides new ways of improving the T_c

of materials [31–33]. In 2007, our group proposed a method based on the structural design of metamaterials for increasing the T_c of superconductors [34,35]. In this method, electroluminescence (EL) materials are directly doped into a superconductor to form a smart meta-superconductor (SMSC). The external field added during the measurement of the T_c of SMSC with a four-probe method can excite the inhomogeneous phases to generate EL, achieving the purpose of strengthening the Cooper pairs, resulting the change of T_c in macroscopic. A SMSC is a material whose T_c can be adjusted and improved by the stimulus of external field, which is a new property and cannot be achieved by traditional doping with a second phase [36–42]. Our group subsequently conducted a series of studies, mainly using MgB_2 as the base superconducting material and Y_2O_3:Eu^{3+} as the base EL material [36–38]. The results obtained in these studies show that unlike conventional chemical doping, which consistently reduces the T_c of MgB_2, the SMSC method of doping EL materials could help increase the T_c of MgB_2. The same conclusions were drawn from substituting the inhomogeneous phase with YVO_4:Eu^{3+} or luminescent nanocomposite Y_2O_3:Eu^{3+}/Ag [39,40] and replacing MgB_2 with Bi(Pb)SrCaCuO [41,42]. The effectiveness of improving the T_c of superconducting materials through the SMSC method by doping with EL inhomogeneous phases has been proven, but the ΔT_c ($\Delta T_c = T_c - T_{cpure}$) values obtained are generally small (0.2–0.4 K). Our previous results show that the SMSC method can only improve T_c at low concentrations of inhomogeneous phases and leads to a small ΔT_c, greatly hindering the further improvement of the T_c of MgB_2. Very recently, our group has increased the T_c of smart meta-superconductor Bi(Pb)SrCaCuO by adjusting the content of inhomogeneous phase [42], implying that the T_c of MgB_2 SMSC can be further improved through the similar method.

In this work, three types of MgB_2 raw materials, namely, $^{a}MgB_2$, $^{b}MgB_2$, and $^{c}MgB_2$, were prepared with particle sizes decreasing in order. Two types of inhomogeneous phases, namely, Y_2O_3:Eu^{3+} and Y_2O_3:Eu^{3+}/Ag, were also prepared based on our previous preparation method [43,44]. Two other types of non-EL dopants, namely, Y_2O_3 and Y_2O_3:Sm^{3+}, were also prepared for comparison. These four types of dopants were incorporated into MgB_2, and the change of T_c was studied. The results show that the T_c of MgB_2 doped with non-EL Y_2O_3 and Y_2O_3:Sm^{3+} was lower than that of pure MgB_2 ($\Delta T_c < 0$). By contrast, EL inhomogeneous phases Y_2O_3:Eu^{3+} and Y_2O_3:Eu^{3+}/Ag increased the T_c ($\Delta T_c > 0$), and the optimal doping concentration of the inhomogeneous phases increased from 0.5% to 1.2% with the decrease of MgB_2's particle size. The optimal doping concentrations for $^{a}MgB_2$, $^{b}MgB_2$, and $^{c}MgB_2$ were 0.5%, 0.8%, and 1.2%, respectively. The corresponding ΔT_{cs} were 0.4 K, 0.9 K, and 1.2 K, which exhibit significant improvements compared with the ΔT_{cs} (0.2–0.4 K) in previous work [36–40]. Such an improvement of T_c is a novel property given that all the experiments before our work confirmed that doping a second phase decreased the T_c of MgB_2.

2. Model

Figure 1a–c show the cross-sectional view of MgB_2 SMSCs models prepared using $^{a}MgB_2$ ($\Phi_a < 30$ μm), $^{b}MgB_2$ ($\Phi_b < 15$ μm), and $^{c}MgB_2$ ($\Phi_c < 5$ μm) as raw materials. Φ_a, Φ_b, and Φ_c refer to the particle sizes of $^{a}MgB_2$, $^{b}MgB_2$, and $^{c}MgB_2$ powders, which will be described in detail at the experiment section. The brown hexagons represent the MgB_2 particles, and the gray dashed lines represent the flakes of inhomogeneous phase with the surface size of approximately 20 nm and thickness of approximately 2.5 nm [40,45]. The flakes of Y_2O_3, Y_2O_3:Sm^{3+}, Y_2O_3:Eu^{3+}, and Y_2O_3:Eu^{3+}/Ag mainly gather on the surfaces of the MgB_2 particles as shown in Figure 1d. Figure 1e–h present the schematics of Y_2O_3, Y_2O_3:Sm^{3+}, Y_2O_3:Eu^{3+}, and Y_2O_3:Eu^{3+}/Ag, respectively. The gray flake represents Y_2O_3. The yellow, white, and green points represent Sm, Eu, and Ag. Obviously, the introduction of these four dopants inevitably reduces the T_c of MgB_2. This is mainly because the dopants are not superconductors, which is unfavorable for the superconductivity of MgB_2, like the impurity phase of MgO in MgB_2. For convenience, the reduction in T_c caused by introducing the dopants is referred to as the impurity effect [36–42]. Non-EL dopants Y_2O_3

and Y_2O_3:Sm^{3+} can only decrease T_c for the introduction of the impurity effect. Unlike Y_2O_3 and Y_2O_3:Sm^{3+}, introducing EL Y_2O_3:Eu^{3+} and Y_2O_3:Eu^{3+}/Ag may increase the T_c, which is referred to as the EL exciting effect [36–42]. Incorporating with inhomogeneous phases has already been confirmed to be an effective method of increasing the T_c for both MgB_2 and Bi(Pb)SrCaCuO systems. The variation of T_c is often associated with the change of electron density. However, in the experiments, the inhomogeneous phases do not react with MgB_2 and the diffusion between the inhomogeneous phases and MgB_2 particles is difficult under the current preparation process and conditions. As a result, the dopants only exist between the MgB_2 particles as shown in Figure 1a–c and cannot change the electron density significantly. Therefore, in principle, the electron density is not the key tuning parameter for the variation of T_c. Although the mechanism for this method remains unclear, we intend to interpret this phenomenon in terms of EL of inhomogeneous phases based on the results of our experiments. During the measurements, the applied external electric field forms local electric fields in the superconductor, which could excite the inhomogeneous phase to produce EL. The generated EL excites the electrons to inject energy, which is favorable to strengthen the Cooper pairs and enables the increase in T_c. However, the completeness of this interpretation needs further demonstration given that the photons may disrupt Cooper pairs. Anyway, further study is required to build a relatively complete theory, especially for such a new experimental phenomenon.

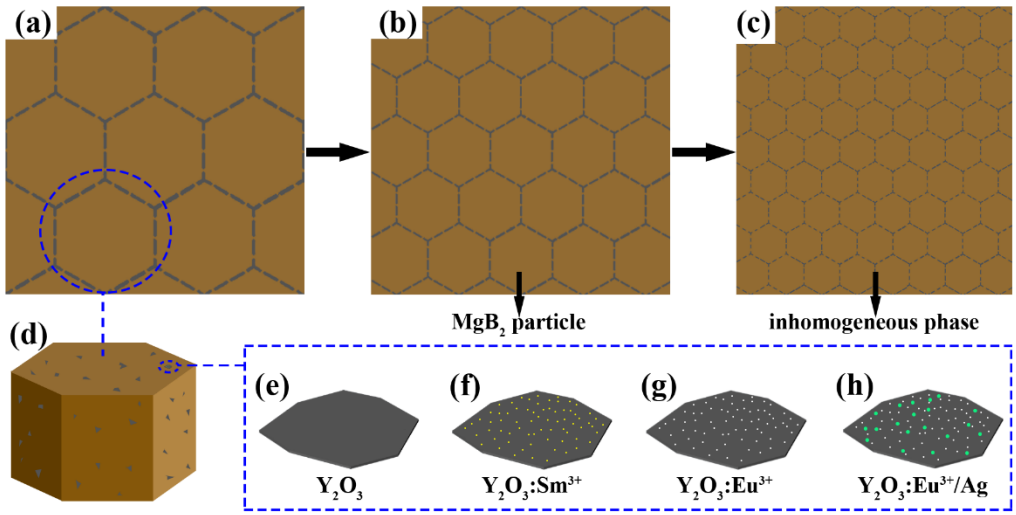

Figure 1. The models of MgB_2 SMSCs prepared using (**a**) $^aMgB_2$ (Φ_a < 30 μm), (**b**) $^bMgB_2$ (Φ_b < 15 μm), and (**c**) $^cMgB_2$ (Φ_c < 5 μm) as raw materials. Schematic depictions of (**d**) a particle of MgB_2 SMSC, (**e**) Y_2O_3, (**f**) Y_2O_3:Sm^{3+}, (**g**) Y_2O_3:Eu^{3+}, and (**h**) Y_2O_3:Eu^{3+}/Ag. The morphology of Y_2O_3, Y_2O_3:Sm^{3+}, Y_2O_3:Eu^{3+}, and Y_2O_3:Eu^{3+}/Ag is flaky with surface size of approximately 20 nm and thickness of approximately 2.5 nm [40].

A distinct competition exists between the impurity effect and EL exciting effect. T_c would be improved ($\Delta T_c > 0$) when EL exciting effect dominates; otherwise, introducing the inhomogeneous phase would decrease T_c ($\Delta T_c < 0$). During the preparation process, the impurity effect should be reduced as extensively as possible, and the EL exciting effect should be enhanced to obtain samples with a high T_c. The resulting superconductor is called a SMSC, and the T_c of which can be improved and adjusted by incorporating EL inhomogeneous phases [36–42], which is a new property and cannot be achieved by traditional doping with a second phase. However, the ΔT_{cs} obtained in our previous work through the SMSC method are quite small. The low doping concentrations of inhomogeneous phases greatly hindered the further improvement of T_c. To further improve the ΔT_c of MgB_2, the doping concentration of the inhomogeneous phase must be increased to enhance the EL exciting effect. However, the impurity effect inevitably increases with the increasing doping concentration, as analyzed above. The results of our previous work show

that the impurity effect tends to dominate at high concentrations, which is not conducive to the T_c of the sample. This phenomenon is principally caused by the agglomeration of excessive inhomogeneous phase flakes, which cannot disperse well in the sample to improve T_c at concentrations exceeding the optimal value. A simple strategy to solve this problem is to reduce the particle size of MgB_2 as shown in Figure 1a–c. It can be seen that reducing the particle size would increase the optimal doping concentration of the inhomogeneous phase. The inhomogeneous phase flakes can disperse well in the sample with small particle size and fully exert the EL exciting effect to further increase ΔT_c. Such a strategy has already been successfully applied to increase the T_c of smart meta-superconductor Bi(Pb)SrCaCuO [42].

3. Experiment

Y_2O_3, Y_2O_3:Sm^{3+}, Y_2O_3:Eu^{3+}, and Y_2O_3:Eu^{3+}/Ag were prepared by a hydrothermal method [40,44]. Briefly, a certain amount of Y_2O_3 and Eu_2O_3 were weighed and dissolved in HCl to make a precursor. The precursor was dissolved in benzyl alcohol and stirred with a magnetic stirrer. A certain amount of octylamine and $AgNO_3$ was added dropwise into the beaker in turn. Then the mixture was transferred to a high-pressure reaction kettle, which was then placed in a drying oven and kept at 250 °C for 24 h. Thereafter, the reaction kettle was naturally cooled to room temperature. The precipitate was washed several times with absolute ethanol to remove impurities and then separated from the solution by centrifugation, precipitation, and drying. The obtained solids were placed in a high-temperature tube furnace and heated at 800 °C for 24 h to form a white powder. After illumination, Y_2O_3:Eu^{3+}/Ag was obtained. The same procedure was carried out prepare Y_2O_3, Y_2O_3:Eu^{3+}, and Y_2O_3:Sm^{3+} by controlling the addition of Eu_2O_3 and $AgNO_3$ and replacing Eu_2O_3 with Sm_2O_3. The morphology of Y_2O_3, Y_2O_3:Sm^{3+}, Y_2O_3:Eu^{3+}, and Y_2O_3:Eu^{3+}/Ag is flaky with surface size of approximately 20 nm and thickness of approximately 2.5 nm [40,45].

Three types of MgB_2 raw materials marked with $^aMgB_2$, $^bMgB_2$, and $^cMgB_2$ were prepared in this work. Φ_a, Φ_b, and Φ_c refer to the particle sizes of $^aMgB_2$, $^bMgB_2$, and $^cMgB_2$ powders. A 500-mesh sieve was used to sift MgB_2 powder (99%, 100 mesh, Alfa Aesar) to prepare $^aMgB_2$, indicating that $\Phi_a < 30$ μm. $^bMgB_2$ was prepared by sifting $^aMgB_2$ powder through vacuum filtration with a pore size of about 15 μm, indicating that $\Phi_b < 15$ μm. Meanwhile, Mg and nano boron powder sifted through vacuum filtration with the pore size of about 5 μm were applied to prepare MgB_2 powder by the traditional sintering process. The obtained MgB_2 powder was then sifted through vacuum filtration with the pore size of about 5 μm to prepare $^cMgB_2$, indicating that $\Phi_c < 5$ μm. MgB_2-based superconductors were synthesized by an ex situ preparation process, which is described in detail in our previous work [37,40]. The doping concentrations in this work all refer to the mass percentage.

4. Results and Discussion

Figure 2a shows the EL spectra of Y_2O_3, Y_2O_3:Sm^{3+}, Y_2O_3:Eu^{3+}, and Y_2O_3:Eu^{3+}/Ag, which confirm that Y_2O_3 and Y_2O_3:Sm^{3+} are non-EL materials, whereas Y_2O_3:Eu^{3+} and Y_2O_3:Eu^{3+}/Ag show a remarkable EL property. Among the four materials tested, Y_2O_3:Eu^{3+}/Ag showed the highest EL intensity because of the composite luminescence [44]. Figure 2b–d present the SEM images of the pure MgB_2 samples prepared using three different raw materials. Figure 2b is the SEM image of $^aMgB_2$, which shows that most of the particle exceeded 1 μm. For $^bMgB_2$, only a few of the particles exceeded 1 μm as shown in Figure 2c. Figure 2d presents the SEM image of $^cMgB_2$, which shows that most of particles are below 500 nm. The particle sizes of $^aMgB_2$, $^bMgB_2$, and $^cMgB_2$ decrease in order. Figure 2e reveals the XRD patterns of four samples. The black and red curves depict the XRD patterns of $^aMgB_2$ and $^aMgB_2$ + 0.5% Y_2O_3:Eu^{3+}/Ag, respectively. The blue and magenta curves correspond to the XRD patterns of $^bMgB_2$ + 0.8% Y_2O_3:Eu^{3+}/Ag and $^cMgB_2$ + 1.2% Y_2O_3:Eu^{3+}/Ag, respectively. The black vertical lines represent the standard XRD patterns

of MgB_2. The main phase of all the samples was clearly MgB_2. The Y_2O_3 phase was found in the doped samples. Small amounts of the unavoidable MgO phase were also detected in all the samples [46–49]. The XRD patterns of the other samples show a similar feature.

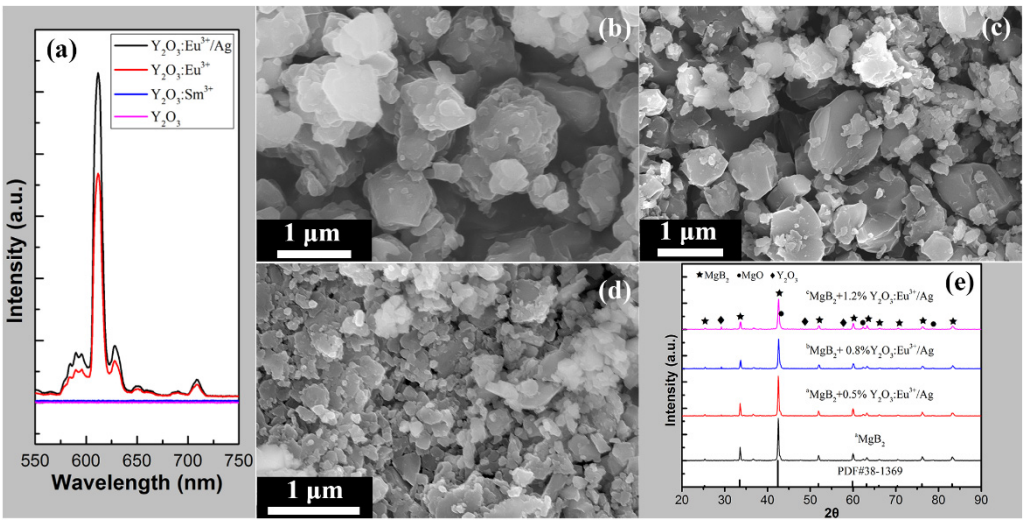

Figure 2. (**a**) EL intensities of Y_2O_3, Y_2O_3:Sm^{3+}, Y_2O_3:Eu^{3+}, and Y_2O_3:Eu^{3+}/Ag. (**b**–**d**) SEM images of $^aMgB_2$, $^bMgB_2$, and $^cMgB_2$. (**e**) XRD patterns of $^aMgB_2$, $^aMgB_2$ + 0.5% Y_2O_3:Eu^{3+}/Ag, $^bMgB_2$ + 0.8% Y_2O_3:Eu^{3+}/Ag, and $^cMgB_2$ + 1.2% Y_2O_3:Eu^{3+}/Ag.

Figure 3a illustrates the normalized resistivity-temperature (R–T) curves of $^aMgB_2$ doped with x% Y_2O_3 (x = 0, 0.2, 0.5, 0.8, 1.0, 1.2). The black curve corresponds to the $^aMgB_2$ sample, which shows that the T_c of the pure sample was 37.4–38.2 K. The other curves represent $^aMgB_2$ doped with Y_2O_3 with concentrations of 0.2%, 0.5%, 0.8%, 1.0%, and 1.2%, indicating that the corresponding T_{cs} are 37.0–37.8 K, 36.8–37.6 K, 36.5–37.3 K, 36.1–37.0 K, and 35.8–36.8 K. The results show that like conventional chemical doping, the introduction of non-EL Y_2O_3 decreases the T_c of MgB_2 ($\Delta T_c < 0$) and tends to increase the superconducting transition width [50]. Meanwhile, the T_{cs} of the doped samples decrease with the increase of the doping concentration as shown in the inset figure. Figure 3b shows the normalized R–T curves of $^aMgB_2$ doped with 0.5% y (y = 0, Y_2O_3, Y_2O_3:Sm^{3+}, Y_2O_3:Eu^{3+}, Y_2O_3:Eu^{3+}/Ag). The doping concentration was fixed at 0.5% base on our previous work [40]. The T_c values of MgB_2 doped with Y_2O_3, Y_2O_3:Sm^{3+}, Y_2O_3:Eu^{3+}, and Y_2O_3:Eu^{3+}/Ag were 36.8–37.6 K, 36.9–37.7 K, 37.6–38.4 K, and 37.8–38.6 K. The results clearly show that non-EL Y_2O_3 and Y_2O_3:Sm^{3+} decreased the T_c of MgB_2, while EL Y_2O_3:Eu^{3+} and Y_2O_3:Eu^{3+}/Ag increased the T_c of MgB_2, as shown in the inset. The T_c values of MgB_2 doped with Y_2O_3:Eu^{3+} and Y_2O_3:Eu^{3+}/Ag increased by 0.2 and 0.4 K, respectively, compared with that of $^aMgB_2$. This finding is similar to those of our previous studies.

Figure 4a illustrates the normalized R–T curves of $^bMgB_2$ doped with x% Y_2O_3:Eu^{3+} (x = 0, 0.5, 0.6, 0.7, 0.8, 1.0). The black curve corresponds to $^bMgB_2$, which shows that the T_c of the pure sample is 36.6–37.4 K. The other curves are the R–T curves of $^bMgB_2$ doped with Y_2O_3:Eu^{3+} with doping concentrations of 0.5%, 0.6%, 0.7%, 0.8%, 0.9%, and 1.0%, indicating that the corresponding T_{cs} are 36.8–37.6 K, 37–37.8 K, 37.2–38.0 K, 37.4–38.2 K, 37.0–37.9 K, and 36.7–37.7 K. The T_c of the doped samples first increased and then decreased with the increase of the doping concentration. The inset summarizes the evolution of ΔT_c as a function of the doping concentration. The optimal doping concentration and the corresponding ΔT_c increased to 0.8% and 0.8 K, respectively, compared with those of the samples prepared using $^aMgB_2$ as raw material. Figure 4b demonstrates the normalized R–T curves of $^bMgB_2$ doped with 0.8% y (y = 0, Y_2O_3, Y_2O_3:Sm^{3+}, Y_2O_3:Eu^{3+}, Y_2O_3:Eu^{3+}/Ag). The T_{cs} of $^bMgB_2$ doped with Y_2O_3, Y_2O_3:Sm^{3+}, Y_2O_3:Eu^{3+}, and Y_2O_3:Eu^{3+}/Ag were 35.8–36.6 K, 36.0–36.8 K, 37.4–38.2 K, and 37.5–38.3 K, respectively. Among these samples,

$^{b}MgB_2$ + 0.8% Y_2O_3:Eu^{3+}/Ag obtained the highest ΔT_c (0.9 K) because of the high EL intensity, as shown in Figure 2a.

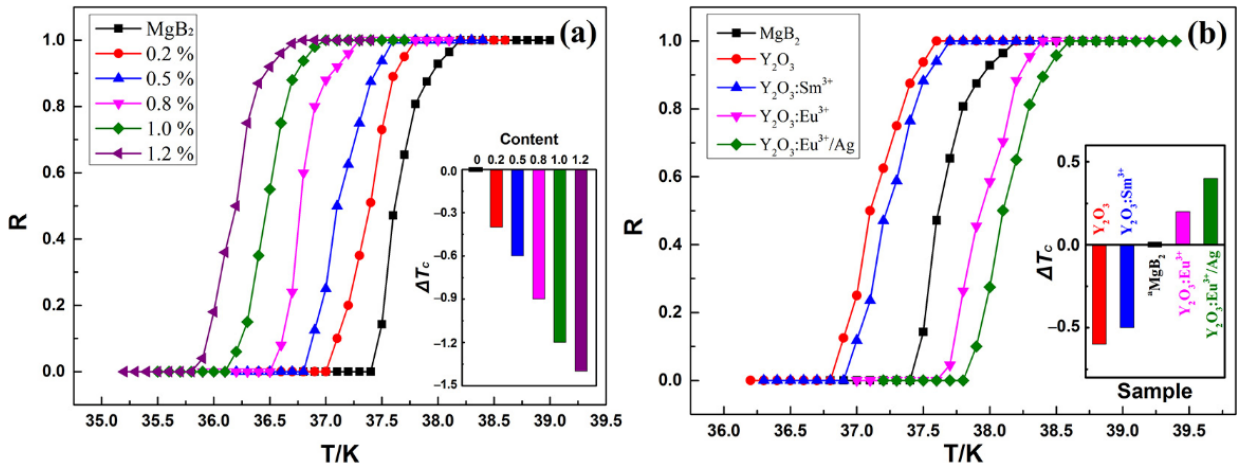

Figure 3. Normalized resistivity-temperature curves of $^{a}MgB_2$ doped with (**a**) x% Y_2O_3 (x = 0, 0.2, 0.5, 0.8, 1.0, 1.2) and (**b**) 0.5% y (y = 0, Y_2O_3, Y_2O_3:Sm^{3+}, Y_2O_3:Eu^{3+}, Y_2O_3:Eu^{3+}/Ag). Insets: the values of ΔT_c ($\Delta T_c = T_c - T_{cpure}$).

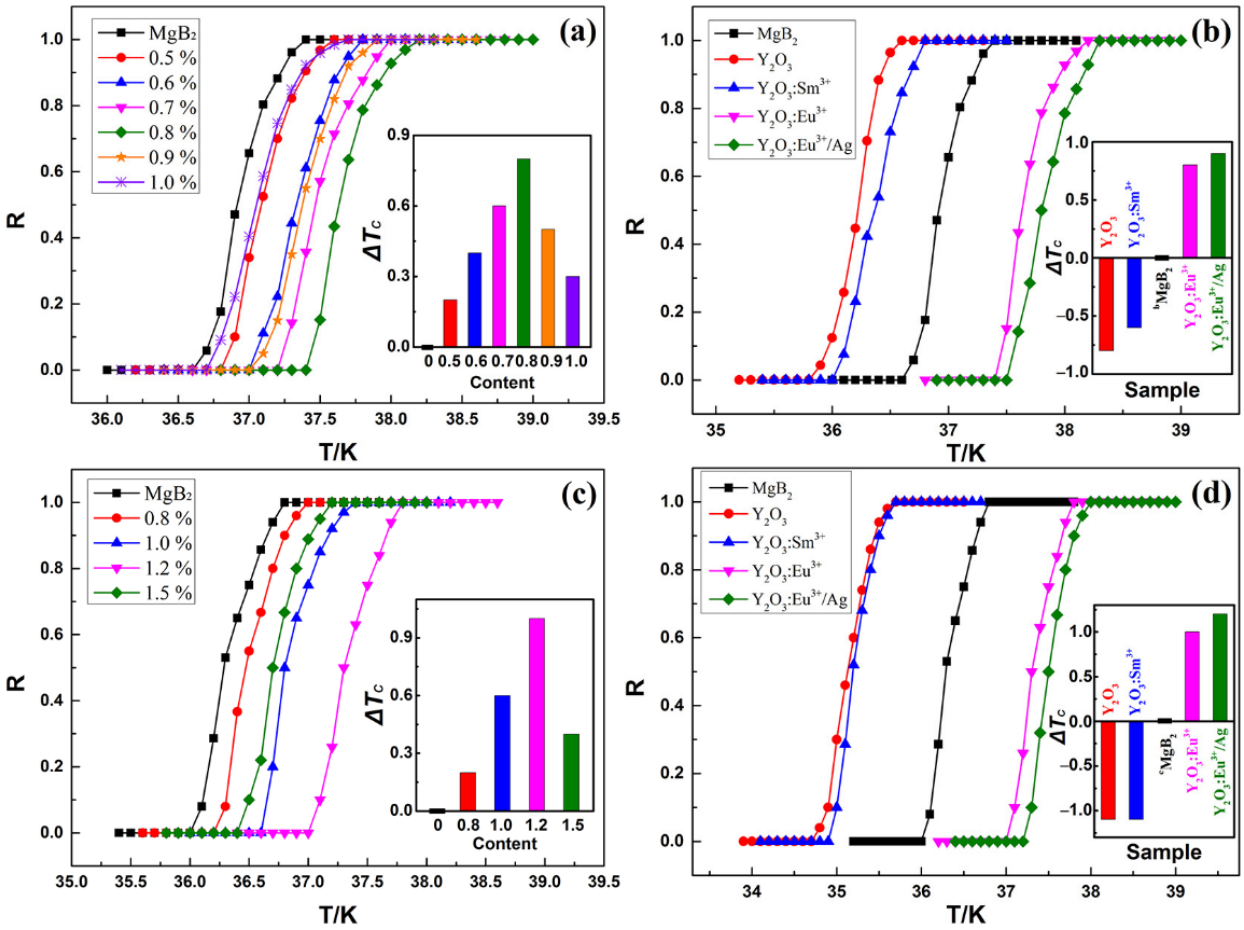

Figure 4. Normalized R–T curves of $^{b}MgB_2$ doped with (**a**) x% Y_2O_3:Eu^{3+} (x = 0, 0.5, 0.6, 0.7, 0.8, 0.9, 1.0) and (**b**) 0.8% y (y = 0, Y_2O_3, Y_2O_3:Sm^{3+}, Y_2O_3:Eu^{3+}, Y_2O_3:Eu^{3+}/Ag). Normalized R–T curves of $^{c}MgB_2$ doped with (**c**) x% Y_2O_3:Eu^{3+} (x = 0, 0.8, 1.0, 1.2, 1.5) and (**d**) 1.2% y (y = 0, Y_2O_3, Y_2O_3:Sm^{3+}, Y_2O_3:Eu^{3+}, Y_2O_3:Eu^{3+}/Ag). Insets: the values of ΔT_c ($\Delta T_c = T_c - T_{cpure}$).

Figure 4c reveals the normalized *R*–*T* curves of $^{c}MgB_2$ doped with *x*% Y_2O_3:Eu^{3+} (*x* = 0, 0.8, 1.0, 1.2, 1.5). Similarly, the black curve corresponds to the pure sample, indicating that the T_c of $^{c}MgB_2$ is 36.0–36.8 K. The other curves correspond to $^{c}MgB_2$ doped with Y_2O_3:Eu^{3+} at different concentrations of 0.8%, 1.0%, 1.2%, and 1.5%, indicating that the corresponding T_{cs} are 36.2–37.0 K, 36.6–37.4 K, 37.0–37.8 K, and 36.4–37.2 K, respectively. It is same with the results in Figure 3a, that is, T_c first increases and then decreases with the increase of the doping concentration, as shown in the inset figure. The optimal doping concentration is 1.2%, and the corresponding ΔT_c is 1.0 K. Figure 4d shows the normalized *R*–*T* curves of $^{c}MgB_2$ doped with 1.2% *y* (*y* = 0, Y_2O_3, Y_2O_3:Sm^{3+}, Y_2O_3:Eu^{3+}, Y_2O_3:Eu^{3+}/Ag). The T_c values of $^{c}MgB_2$ doped with Y_2O_3, Y_2O_3:Sm^{3+}, Y_2O_3:Eu^{3+}, Y_2O_3:Eu^{3+}/Ag are 34.7–35.7 K, 34.9–35.7 K, 37.0–37.8 K, and 37.2–38.0 K. Y_2O_3 and Y_2O_3:Sm^{3+} decrease T_c, whereas Y_2O_3:Eu^{3+} and Y_2O_3:Eu^{3+}/Ag increase T_c. These results are consistent with those of the samples prepared using $^{a}MgB_2$ and $^{b}MgB_2$ as raw materials. The T_c of $^{c}MgB_2$ + 1.2% Y_2O_3:Eu^{3+}/Ag was enhanced by 1.2 K compared with that of the pure sample, exhibiting the highest ΔT_c among the samples.

Figure 5a shows the SEM image of $^{a}MgB_2$ + 0.5% Y_2O_3:Eu^{3+}/Ag. Figure 5b–e are the EDS mapping for elements Mg, Y, Eu, and Ag listed in the lower right corner of each figure. Figure 5h shows the SEM image of $^{c}MgB_2$ + 1.2% Y_2O_3:Eu^{3+}/Ag. Figure 5g–j are the EDS mapping for elements Mg, Y, Eu, and Ag. Given that the inhomogeneous phase did not react with MgB_2, the mapping of elements Y, Eu, and Ag can reflect the distribution of the inhomogeneous phase in the sample. It can be seen that Y_2O_3:Eu^{3+}/Ag is relatively evenly distributed in $^{a}MgB_2$. Similarly, the inhomogeneous phase did not generate significant agglomeration in $^{c}MgB_2$, even though the optimal concentration was enhanced to 1.2% as the particle size decreased, as shown in Figure 5g–j. Therefore, the inhomogeneous phase was able to fully exert the EL exciting effect to further increase ΔT_c at high concentrations.

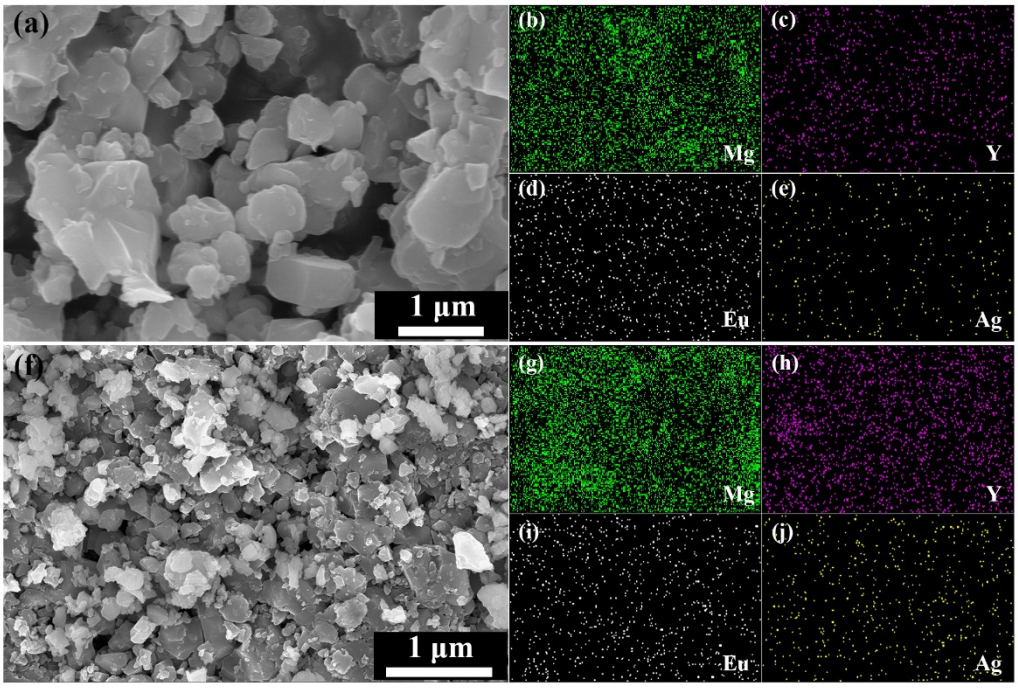

Figure 5. (**a**) SEM image and (**b**–**e**) EDS mapping of $^{a}MgB_2$ + 0.5% Y_2O_3:Eu^{3+}/Ag. (**f**) SEM image and (**g**–**j**) EDS mapping of $^{c}MgB_2$ + 1.2% Y_2O_3:Eu^{3+}/Ag.

Table 1 shows the ΔT_{cs} for $^{a}MgB_2$ + 0.5% *x*, $^{b}MgB_2$ + 0.8% *x*, and $^{c}MgB_2$ + 1.2% *x* (*x* = Y_2O_3, Y_2O_3:Sm^{3+}, Y_2O_3:Eu^{3+}, and Y_2O_3:Eu^{3+}/Ag). For the three kinds of MgB_2 raw materials, non-EL dopants Y_2O_3 and Y_2O_3:Sm^{3+} can only decrease T_c ($\Delta T_c < 0$) and the higher the doping concentration, the lower the T_c. However, EL inhomogeneous phases can increase the T_c ($\Delta T_c > 0$). For the $^{a}MgB_2$ raw material, we prepared the MgB_2 SMSCs

doped with 0.5% inhomogeneous phase. The results show that ΔT_c values for $^{a}MgB_2$ doped with Y_2O_3:Eu^{3+} and Y_2O_3:Eu^{3+}/Ag are 0.2 K and 0.4 K. For the $^{b}MgB_2$ raw material with a smaller particle size than that of $^{a}MgB_2$, the optimal doping concentration was first explored by changing the concentration of Y_2O_3:Eu^{3+} from 0.5% to 1.0%. The results show that the optimal doping concentration is 0.8%. Subsequently, 0.8% Y_2O_3:Eu^{3+}, and Y_2O_3:Eu^{3+}/Ag were separately doped into $^{b}MgB_2$ and the corresponding ΔT_c values were 0.8 K and 0.9 K, respectively. Similar results were obtained in the samples prepared using $^{c}MgB_2$ as the raw material. For $^{c}MgB_2$, which has the smallest particle size among the three raw materials, the optimal concentration was enhanced to 1.2%. The ΔT_{cs} for $^{c}MgB_2$ doped with Y_2O_3:Eu^{3+} and Y_2O_3:Eu^{3+}/Ag were 1.0 K and 1.2 K, respectively. These results indicate that reducing the particle size can effectively increase the optimal doping concentration of the inhomogeneous phase, thereby enhancing the ΔT_c.

Table 1. ΔT_{cs} for $^{a}MgB_2$ + 0.5% x, $^{b}MgB_2$ + 0.8% x and $^{c}MgB_2$ + 1.2% x (x = Y_2O_3, Y_2O_3:Sm^{3+}, Y_2O_3:Eu^{3+}, and Y_2O_3:Eu^{3+}/Ag).

ΔT_{cs}	Y_2O_3	Y_2O_3:Sm^{3+}	Y_2O_3:Eu^{3+}	Y_2O_3:Eu^{3+}/Ag
$^{a}MgB_2$ (0.5%)	−0.6 K	−0.5 K	0.2 K	0.4 K
$^{b}MgB_2$ (0.8%)	−0.8 K	−0.6 K	0.8 K	0.9 K
$^{c}MgB_2$ (1.2%)	−1.1 K	−1.1 K	1.0 K	1.2 K

In this work, the ΔT_c is improved by increasing the optimal doping concentration of inhomogeneous phases through reducing the particle size, however, the T_c values of MgB_2 SMSCs are relatively low due to the low T_c of the pure MgB_2 sample. As the particle size decreases, the grain boundaries in the sample increase and the connectivity decreases, which are disadvantages to the superconductivity [51–53]. One possible solution is to incorporate the inhomogeneous phase into the interior of the particles to overcome the disadvantages caused by the increasing grain boundaries with the doping concentration increasing.

5. Conclusions

Although the effectiveness of improving the T_c of superconducting materials through the SMSC method by doping with EL inhomogeneous phases has been proven in previous works, the ΔT_{cs} obtained are quite small. To further increase ΔT_c, three types of MgB_2 raw materials, namely, $^{a}MgB_2$, $^{b}MgB_2$, and $^{c}MgB_2$, were prepared with particle sizes decreasing in order. EL inhomogeneous phases were incorporated into these three raw materials with different concentrations to study the change of ΔT_c. The results show that the optimal doping concentrations for $^{a}MgB_2$, $^{b}MgB_2$, and $^{c}MgB_2$ are 0.5%, 0.8%, and 1.2%, respectively. The corresponding ΔT_{cs} are 0.4, 0.9, and 1.2 K, respectively. Meanwhile, increasing the EL intensity of the inhomogeneous phase can be considered to further increase ΔT_c. This work not only proves the effectiveness of the SMSC method in improving T_c but also provides an alternative approach to improving the T_c of superconducting materials.

Author Contributions: Conceptualization, X.Z.; methodology, X.Z. and Y.L.; software, Y.L., G.H.; validation, X.Z., Y.L. and G.H.; formal analysis, X.Z., Y.L., G.H., H.Z., L.T. and H.C.; investigation, Y.L., G.H., H.Z., L.T. and H.C.; resources, X.Z.; data curation, Y.L., G.H., H.Z., L.T. and H.C.; writing—original draft preparation, Y.L.; writing—review and editing, X.Z. and Y.L.; visualization, X.Z. and Y.L.; supervision, X.Z.; project administration, X.Z.; funding acquisition, X.Z. All authors have read and agreed to the published version of the manuscript.

Funding: This research was funded by the National Natural Science Foundation of China for Distinguished Young Scholar, grant number 50025207.

Institutional Review Board Statement: Not applicable.

Informed Consent Statement: Not applicable.

Data Availability Statement: The data presented in this study are available on request from the corresponding author.

Conflicts of Interest: The authors declare no conflict of interest. The funders had no role in the design of the study; in the collection, analyses, or interpretation of data; in the writing of the manuscript, or in the decision to publish the results.

References

1. Bardeen, J.; Cooper, L.N.; Schrieffer, J.R. Theory of Superconductivity. *Phys. Rev.* **1957**, *108*, 1175–1204. [CrossRef]
2. McMillan, W.L. Transition Temperature of Strong-Coupled Superconductors. *Phys. Rev.* **1968**, *167*, 331–344. [CrossRef]
3. Bednorz, J.G.; Müller, K.A. Possible high T_c superconductivity in the Ba-La-Cu-O system. *Z. Phys. B-Condens. Matter* **1986**, *64*, 189–193. [CrossRef]
4. Mohd Yusuf, N.; Awang Kechik, M.; Baqiah, H.; Soo Kien, C.; Kean Pah, L.; Shaari, A.; Wan Jusoh, W.; Abd Sukor, S.; Mousa Dihom, M.; Talib, Z.; et al. Structural and Superconducting Properties of Thermal Treatment-Synthesised Bulk $YBa_2Cu_3O_{7-\delta}$ Superconductor: Effect of Addition of SnO_2 Nanoparticles. *Materials* **2018**, *12*, 92. [CrossRef] [PubMed]
5. Kamihara, Y.; Watanabe, T.; Hirano, M.; Hosono, H. Iron-Based Layered Superconductor $La[O_{1-X}F_X]FeAs$ (x = 0.05–0.12) with T_c = 26 K. *J. Am. Chem. Soc.* **2008**, *130*, 3296–3297. [CrossRef]
6. Zhang, P.; Yaji, K.; Hashimoto, T.; Ota, Y.; Kondo, T.; Okazaki, K.; Wang, Z.; Wen, J.; Gu, G.D.; Ding, H.; et al. Observation of topological superconductivity on the surface of an iron-based superconductor. *Science* **2018**, *360*, 182–186. [CrossRef]
7. Drozdov, A.P.; Eremets, M.I.; Troyan, I.A.; Ksenofontov, V.; Shylin, S.I. Conventional superconductivity at 203 kelvin at high pressures in the sulfur hydride system. *Nature* **2015**, *525*, 73–76. [CrossRef]
8. Cantaluppi, A.; Buzzi, M.; Jotzu, G.; Nicoletti, D.; Mitrano, M.; Pontiroli, D.; Ricco, M.; Perucchi, A.; Di Pietro, P.; Cavalleri, A. Pressure tuning of light-induced superconductivity in K_3C_{60}. *Nat. Phys.* **2018**, *14*, 837–841. [CrossRef]
9. Drozdov, A.P.; Kong, P.P.; Minkov, V.S.; Besedin, S.P.; Kuzovnikov, M.A.; Mozaffari, S.; Balicas, L.; Balakirev, F.F.; Graf, D.E.; Prakapenka, V.B.; et al. Superconductivity at 250 K in lanthanum hydride under high pressures. *Nature* **2019**, *569*, 528–531. [CrossRef]
10. Snider, E.; Dasenbrock-Gammon, N.; McBride, R.; Debessai, M.; Vindana, H.; Vencatasamy, K.; Lawler, K.V.; Salamat, A.; Dias, R.P. Room-temperature superconductivity in a carbonaceous sulfur hydride. *Nature* **2020**, *586*, 373–377. [CrossRef] [PubMed]
11. Fausti, D.; Tobey, R.I.; Dean, N.; Kaiser, S.; Dienst, A.; Hoffmann, M.C.; Pyon, S.; Takayama, T.; Takagi, H.; Cavalleri, A. Light-induced superconductivity in a stripe-ordered cuprate. *Science* **2011**, *331*, 189–191. [CrossRef] [PubMed]
12. Cavalleri, A. Photo-induced superconductivity. *Contemp. Phys.* **2017**, *59*, 31–46. [CrossRef]
13. Nagamatsu, J.; Nakagawa, N.; Muranaka, T.; Zenitani, Y.; Akimitsu, J. Superconductivity at 39 K in magnesium diboride. *Nature* **2001**, *410*, 63–64. [CrossRef]
14. Bohnen, K.P.; Heid, R.; Renker, B. Phonon dispersion and electron-phonon coupling in MgB_2 and AlB_2. *Phys. Rev. Lett.* **2001**, *86*, 5771–5774. [CrossRef] [PubMed]
15. Buzea, C.; Yamashita, T. Review of the superconducting properties of MgB_2. *Supercond. Sci. Technol.* **2001**, *14*, R115–R146. [CrossRef]
16. Yildirim, T.; Gulseren, O.; Lynn, J.W.; Brown, C.M.; Udovic, T.J.; Huang, Q.; Rogado, N.; Regan, K.A.; Hayward, M.A.; Slusky, J.S.; et al. Giant anharmonicity and nonlinear electron-phonon coupling in MgB_2: A combined first-principles calculation and neutron scattering study. *Phys. Rev. Lett.* **2001**, *87*, 037001. [CrossRef] [PubMed]
17. Singh, P.P. From E_{2g} to other modes: Effects of pressure on electron-phonon interaction in MgB_2. *Phys. Rev. Lett.* **2006**, *97*, 247002. [CrossRef]
18. Vinod, K.; Varghese, N.; Syamaprasad, U. Superconductivity of MgB_2 in the BCS framework with emphasis on extrinsic effects on critical temperature. *Supercond. Sci. Technol.* **2007**, *20*, R31–R45. [CrossRef]
19. Varilci, A.; Yegen, D.; Tassi, M.; Stamopoulos, D.; Terzioglu, C. Effect of annealing temperature on some physical properties of MgB_2 by using the Hall probe ac-susceptibility method. *Phys. B: Condens. Matter* **2009**, *404*, 4054–4059. [CrossRef]
20. Zhao, Y.G.; Zhang, X.P.; Qiao, P.T.; Zhang, H.T.; Jia, S.L.; Cao, B.S.; Zhu, M.H.; Han, Z.H.; Wang, X.L.; Gu, B.L. Effect of Li doping on structure and superconducting transition temperature of $Mg_{1-x}Li_xB_2$. *Phys. C* **2001**, *361*, 91–94. [CrossRef]
21. Mackinnon, I.D.R.; Winnett, A.; Alarco, J.A.; Talbot, P.C. Synthesis of MgB_2 at low temperature and autogenous pressure. *Materials* **2014**, *7*, 3901–3918. [CrossRef] [PubMed]
22. Ozturk, O.; Asikuzun, E.; Kaya, S.; Koc, N.S.; Erdem, M. The effect of Ar ambient pressure and annealing duration on the cicrostructure, superconducting properties and activation energies of MgB_2 superconductors. *J. Supercond. Nov. Magn.* **2016**, *30*, 1161–1169. [CrossRef]
23. Cheng, F.; Ma, Z.; Liu, C.; Li, H.; Shahriar, A.; Hossain, M.; Bando, Y.; Yamauchi, Y.; Fatehmulla, A.; Farooq, W.A.; et al. Enhancement of grain connectivity and critical current density in the ex-situ sintered MgB_2 superconductors by doping minor Cu. *J. Alloys Compd.* **2017**, *727*, 1105–1109. [CrossRef]
24. Grivel, J.C.; Rubešová, K. Increase of the critical current density of MgB_2 superconducting bulk samples by means of methylene blue dye additions. *Phys. C* **2019**, *565*, 1353506. [CrossRef]
25. Li, S.Y.; Xiong, Y.M.; Mo, W.Q.; Fan, R.; Wang, C.H.; Luo, X.G.; Sun, Z.; Zhang, H.T.; Li, L.; Cao, L.Z.; et al. Alkali metal substitution efffects in $Mg_{1-x}A_xB_2$ (A = Li and Na). *Phys. C* **2001**, *363*, 219–223. [CrossRef]

26. Slusky, J.S.; Rogado, N.; Regan, K.A.; Hayward, M.A.; Khalifah, P.; He, T.; Inumaru, K.; Loureiro, S.M.; Haas, M.K.; Zandbergen, H.W.; et al. Loss of superconductivity with the addition of Al to MgB_2 and a structural transition in $Mg_{1-x}Al_xB_2$. *Nature* **2001**, *410*, 343. [CrossRef] [PubMed]
27. Dou, S.X.; Soltanian, S.; Horvat, J.; Wang, X.L.; Zhou, S.H.; Ionescu, M.; Liu, H.K. Enhancement of the critical current density and flux pinning of MgB_2 superconductor by nanoparticle SiC doping. *Appl. Phys. Lett.* **2002**, *81*, 3419–3421. [CrossRef]
28. Li, G.Z.; Sumption, M.D.; Rindfleisch, M.A.; Thong, C.J.; Tomsic, M.J.; Collings, E.W. Enhanced higher temperature (20–30 K) transport properties and irreversibility field in nano-Dy_2O_3 doped advanced internal Mg infiltration processed MgB_2 composites. *Appl. Phys. Lett.* **2014**, *105*, 112603. [CrossRef]
29. Susner, M.A.; Bohnenstiehl, S.D.; Dregia, S.A.; Sumption, M.D.; Yang, Y.; Donovan, J.J.; Collings, E.W. Homogeneous carbon doping of magnesium diboride by high-temperature, high-pressure synthesis. *Appl. Phys. Lett.* **2014**, *104*, 162603. [CrossRef]
30. Shahabuddin, M.; Madhar, N.A.; Alzayed, N.S.; Asif, M. Uniform dispersion and exfoliation of multi-walled carbon nanotubes in CNT-MgB_2 superconductor composites using surfactants. *Materials* **2019**, *12*, 3044. [CrossRef]
31. Liu, H.; Zhao, X.P.; Yang, Y.; Li, Q.W.; Lv, J. Fabrication of infrared left-handed metamaterials via double template-assisted electrochemical deposition. *Adv. Mater.* **2008**, *20*, 2050–2054. [CrossRef]
32. Smolyaninova, V.N.; Zander, K.; Gresock, T.; Jensen, C.; Prestigiacomo, J.C.; Osofsky, M.S.; Smolyaninov, I.I. Using metamaterial nanoengineering to triple the superconducting critical temperature of bulk aluminum. *Sci. Rep.* **2015**, *5*, 15777. [CrossRef] [PubMed]
33. Smolyaninov, I.I.; Smolyaninova, V.N. Theoretical modeling of critical temperature increase in metamaterial superconductors. *Phys. Rev. B* **2016**, *93*, 184510. [CrossRef]
34. Jiang, W.T.; Xu, Z.L.; Chen, Z.; Zhao, X.P. Introduce uniformly distributed ZnO nano-defects into BSCCO superconductors by nano-composite method. *J. Funct. Mater.* **2007**, *38*, 157–160. Available online: http://www.cnki.com.cn/Article/CJFDTOTAL-GNCL200701046.htm (accessed on 30 April 2021). (In Chinese).
35. Xu, S.H.; Zhou, Y.W.; Zhao, X.P. Research and development of inorganic powder EL materials. *Mater. Rep.* **2007**, *21*, 162–166. Available online: http://www.cnki.com.cn/Article/CJFDTotal-CLDB2007S3048.htm (accessed on 30 April 2021). (In Chinese).
36. Zhang, Z.W.; Tao, S.; Chen, G.W.; Zhao, X.P. Improving the critical temperature of MgB_2 superconducting metamaterials induced by electroluminescence. *J. Supercond. Nov. Magn.* **2016**, *29*, 1159–1162. [CrossRef]
37. Tao, S.; Li, Y.B.; Chen, G.W.; Zhao, X.P. Critical temperature of smart meta-superconducting MgB_2. *J. Supercond. Nov. Magn.* **2017**, *30*, 1405–1411. [CrossRef]
38. Chen, H.G.; Li, Y.B.; Chen, G.W.; Xu, L.X.; Zhao, X.P. The effect of inhomogeneous phase on the critical temperature of smart meta-superconductor MgB_2. *J. Supercond. Nov. Magn.* **2018**, *31*, 3175–3182. [CrossRef]
39. Li, Y.B.; Chen, H.G.; Qi, W.C.; Chen, G.W.; Zhao, X.P. Inhomogeneous phase effect of smart meta-superconducting MgB_2. *J. Low. Temp. Phys.* **2018**, *191*, 217–227. [CrossRef]
40. Li, Y.B.; Chen, H.G.; Wang, M.Z.; Xu, L.X.; Zhao, X.P. Smart meta-superconductor MgB_2 constructed by the dopant phase of luminescent nanocomposite. *Sci. Rep.* **2019**, *9*, 14194. [CrossRef]
41. Chen, H.G.; Li, Y.B.; Wang, M.Z.; Han, G.Y.; Shi, M.; Zhao, X.P. Smart metastructure method for increasing T_c of Bi(Pb)SrCaCuO high-temperature superconductors. *J. Supercond. Nov. Magn.* **2020**, *33*, 3015–3025. [CrossRef]
42. Chen, H.G.; Wang, M.Z.; Qi, Y.; Li, Y.B.; Zhao, X.P. Relationship between the T_C of Smart Meta-Superconductor Bi(Pb)SrCaCuO and Inhomogeneous Phase Content. *Nanomaterials* **2021**, *11*, 1061. [CrossRef]
43. Chen, G.W.; Qi, W.C.; Li, Y.B.; Yang, C.S.; Zhao, X.P. Hydrothermal synthesis of Y_2O_3:Eu^{3+} nanorods and its growth mechanism and luminescence properties. *J. Mater. Sci. Mater. Electron.* **2016**, *27*, 5628–5634. [CrossRef]
44. Wang, M.Z.; Xu, L.X.; Chen, G.W.; Zhao, X.P. Topological luminophor Y_2O_3:Eu^{3+}+Ag with high electroluminescence performance. *ACS Appl. Mater. Interfaces* **2019**, *11*, 2328–2335. [CrossRef]
45. Xu, L.X.; Wang, M.Z.; Liu, Z.X.; Zhao, X.P. Nano-topological luminophor Y_2O_3:Eu^{3+} + Ag with concurrent photoluminescence and electroluminescence. *J. Mater. Sci. Mater. Electron.* **2019**, *30*, 20243–20252. [CrossRef]
46. Eyidi, D.; Eibl, O.; Wenzel, T.; Nickel, K.G.; Giovannini, M.; Saccone, A. Phase analysis of superconducting polycrystalline MgB_2. *Micron* **2003**, *34*, 85–96. [CrossRef]
47. Shi, Q.Z.; Liu, Y.C.; Gao, Z.M.; Zhao, Q. Formation of MgO whiskers on the surface of bulk MgB_2 superconductors during in situ sintering. *J. Mater. Sci.* **2007**, *43*, 1438–1443. [CrossRef]
48. Ma, Z.Q.; Liu, Y.C.; Shi, Q.Z.; Zhao, Q.; Gao, Z.M. The improved superconductive properties of MgB_2 bulks with minor Cu addition through reducing the MgO impurity. *Phys. C* **2008**, *468*, 2250–2253. [CrossRef]
49. Singh, D.K.; Tiwari, B.; Jha, R.; Kishan, H.; Awana, V.P.S. Role of MgO impurity on the superconducting properties of MgB_2. *Phys. C* **2014**, *505*, 104–108. [CrossRef]
50. Wang, C.C.; Zeng, R.; Xu, X.; Dou, S.X. Superconducting transition width under magnetic field in MgB_2 polycrystalline samples. *J. Appl. Phys.* **2010**, *108*, 093907. [CrossRef]
51. Dogruer, M.; Yildirim, G.; Ozturk, O.; Terzioglu, C. Analysis of indentation size effect on mechanical properties of Cu-diffused bulk MgB_2 superconductor using experimental and different theoretical models. *J. Supercond. Nov. Magn.* **2012**, *26*, 101–109. [CrossRef]

52. Mizutani, S.; Yamamoto, A.; Shimoyama, J.-I.; Ogino, H.; Kishio, K. Self-sintering-assisted high intergranular connectivity in ball-milled ex situ MgB_2 bulks. *Supercond. Sci. Technol.* **2014**, *27*, 114001. [CrossRef]
53. Ozturk, O.; Asikuzun, E.; Kaya, S. Significant change in micro mechanical, structural and electrical properties of MgB_2 superconducting ceramics depending on argon ambient pressure and annealing duration. *J. Mater. Sci. Mater. Electron.* **2015**, *26*, 3840–3852. [CrossRef]